

Dimensional cross-over of hard parallel cylinders confined on cylindrical surfaces

Yuri Martínez-Ratón*

*Grupo Interdisciplinar de Sistemas Complejos (GISC), Departamento de Matemáticas,
Escuela Politécnica Superior, Universidad Carlos III de Madrid,
Avenida de la Universidad 30, E-28911, Leganés, Madrid, Spain*

Enrique Velasco†

*Departamento de Física Teórica de la Materia Condensada
and Instituto de Ciencia de Materiales Nicolás Cabrera,
Universidad Autónoma de Madrid, E-28049 Madrid, Spain*

(Dated: September 21, 2018)

Abstract

We derive, from the dimensional cross-over criterion, a fundamental-measure density functional for parallel hard curved rectangles moving on a cylindrical surface. We derive it from the density functional of circular arcs of length σ with centers of mass located on an external circumference of radius R_0 . The latter functional in turns is obtained from the corresponding 2D functional for a fluid of hard discs of radius R on a flat surface with centers of mass confined onto a circumference of radius R_0 . Thus the curved length of closest approach between two centers of mass of hard discs on this circumference is $\sigma = 2R_0 \sin^{-1}(R/R_0)$, the length of the circular arcs. From the density functional of circular arcs, and by applying a dimensional expansion procedure to the spatial dimension orthogonal to the plane of the circumference, we finally obtain the density functional of curved rectangles of edge-lengths σ and L . The DF for curved rectangles can also be obtained by fixing the centers of mass of parallel hard cylinders of radius R and length L on a cylindrical surface of radius R_0 . Along the derivation, we show that when the centers of mass of the discs are confined to the exterior circumference of a circle of radius R_0 : (i) for $R_0 > R$, the exact Percus 1D-density functional of circular arcs of length $2R_0 \sin^{-1}(R/R_0)$ is obtained, and (ii) for $R_0 < R$, the 0D limit (a cavity that can hold one particle at most) is recovered. We also show that, for $R_0 > R$, the obtained functional is equivalent to that of parallel hard rectangles on a flat surface of the same lengths, except that now the density profile of curved rectangles is a periodic function of the azimuthal angle, $\rho(\phi, z) = \rho(\phi + 2\pi, z)$. The phase behavior of a fluid of aligned curved rectangles is obtained by calculating the free-energy branches of smectic, columnar and crystalline phases for different values of the ratio R_0/R in the range $1 < R_0/R \leq 4$; the smectic phase turns out to be the most stable except for $R_0/R = 4$ where the crystalline phase becomes reentrant in a small range of packing fractions. When $R_0/R < 1$ the transition is absent, since the density functional of curved rectangles reduces to the 1D Percus functional.

PACS numbers: 61.20.Gy, 61.30.Cz, 64.75.+g

*Electronic address: yuri@math.uc3m.es

†Electronic address: enrique.velasco@uam.es

I. INTRODUCTION

The subjects of surfaces decorated with particles in periodically or quasiperiodically packed configurations and the arrangement of spheres on spherical, cylindrical or general surfaces have attracted a long-standing interest [1, 2]. The focus has been mainly on the type of packing, defect stabilisation and interactions, and the topological constraints associated with non-vanishing Gaussian curvature. A most prominent problem concerns the stabilisation of crystalline order on a sphere, first predicted [3] and then experimentally observed in colloidal spheres on water droplets [4]. The problem has many important consequences in a number of fields; for example, possible packings of protein capsomeres in spherical viruses [5], behaviour of particles inserted in lipid membranes and their curvature-induced interactions [6, 7], metallic clusters, structure of fullerenes, to name just a few. The spherical or effectively spherical surface is the most studied, while several studies have also appeared on cylindrical surfaces. Recently, Nelson studied the interaction of dislocations on a cylindrical surface [8]; despite the vanishing Gaussian curvature of the cylinder, a rich phenomenology was found.

Of particular interest is the case when particles are not spherical but elongated, since here there are issues of packing not only from the translational but also from the orientational degrees of freedom. Hence one has here two fields, the position and the nematic-director fields, that compete and interact with the geometry to possibly stabilise complex defect patterns. In a nematic phase particle positions are disordered but the nematic director is still constrained by the topology. The possibility of stabilising defects by confining a thin nematic film on a spherical surface is intriguing. For example, using computer simulation, Dzubiella et al. [9] studied the nematic ordering of hard rods confined to be on the surface of a sphere. In this case the confinement on a spherical surface induces a global topological charge in the director field due to the stabilisation of half-integer topological point defects.

Another interesting, much less analysed, aspect, concerns the formation of phases with partial positional order (liquid-crystalline) from a disordered phase and the conditions imposed by topology, curvature and periodicity on the ordering and phase interplay as thermodynamic conditions (such as surface density of particles or temperature) are varied. In liquid-crystalline phases with partial or total translational order (smectic, columnar or crystalline) the two fields are coupled, and a complex interaction with the topology may result.

This problem may be relevant in connection with the ordering of large protein molecules inserted into lipid membranes, where curvature may both induce or modify order and be induced or modified by order.

In the present article we focus on a system of parallel circular, rectangular particles confined to a cylindrical surface (therefore the nematic phase is the most disordered phase of the system). This is motivated as a useful model to discuss ordering of squared or rectangular proteins or otherwise on rod-shaped bacterial cell membranes, but the model can be analysed in a broader context. Despite its simple topology, the non-vanishing curvature and periodicity perpendicular to the cylinder axis may induce or suppress ordering in some of the two orthogonal directions, giving rise to possible smectic or columnar orderings of the particles on the cylindrical surface. This problem has some similarities with the adsorption of particles *inside* slit-like or cylindrical pores (an example of which is the recent study on the confinement of hard spheres (HS) into cylindrical pores [10], or of hard rods into planar pores [12, 13], both employing the density-functional (DF) formalism). Recently the close-packed structures of HS confined in cylindrical pores of small radii were classified using analytical methods and computer simulations [14]. All of these studies reflect the importance of the commensuration between the pore width (in our case the circle diameter) and the characteristic dimensions of particles in the structure and stability of the confined non-uniform phases. Recent studies show that the extreme confinement of particles along one direction makes the system behave like an ideal gas in this direction. Thus the corresponding degrees of freedom can be integrated out and the resulting lower-dimensional system can be described by an effective interparticle potential [11].

The purpose of the present article is twofold. First, we derive a density-functional theory for a fluid of parallel circular rectangles on an external cylindrical surface; this model is isomorphic to a fluid monolayer of parallel cylinders adsorbed on an external cylindrical surface, or to the same fluid confined between two concentric cylindrical surfaces such that only one shell of cylinders can be accommodated with no radial motion. We show that the functional may be obtained consistently from different routes due to the important dimensional-crossover property of the theory. This property was first used to derive a fundamental measure density functional (FMD) for HS [15, 16] and parallel hard cubes (PHC) [17], and it was recently applied to obtain a density functional for hard parallel cylinders [18]. Second, the model is analysed statistically-mechanically by investigating the free-energy

minima landscape. We discuss different régimes for the ratio of radius of the external cylinder to radii of the underlying adsorbed cylinders. When the ratio is sufficiently low the model is an effectively 1D model and no phase transition exists. Otherwise the smectic phase is found to be the most stable except for a relative small range of densities in which the crystalline phase appears as a reentrant phase. These results are in line with those of recent experiments on confined liquid crystals in silica-glass nanochannels, which show that the stability of the smectic phase is considerably enhanced by the confinement at the expense of the crystalline phase [19]. We finally propose, following the dimensional cross-over property, a DF for spherical lenses (the intersection between a HS of radius R which center of mass is located on an external sphere of radius R_0 , with $R_0 > R$) moving on a spherical surface.

The article is arranged as follows. In Section II we derive the density-functional theory for hard curved rectangles (CR) on an external cylindrical surface. This is done in two steps: in the first (Section II A), the 2D functional for hard discs (HD) is projected on the surface of an external circle, thus obtaining a 1D functional for curved arcs (CA) that move along the circumference of the external circle. In the second (Section II B) the functional is developed along the direction perpendicular to the circle to give a 2D functional for CR. Dimensional consistency is discussed in Section II C. The results are presented in Section III. In Section V we propose, following the same dimensional cross-over recipe, a DF for spherical lenses which center of mass are confined on a external sphere. Finally some conclusions are presented in Section VI. Details on the derivation of the density functionals and the density profile parameterizations are relegated to Appendices A-C.

II. DERIVATION OF FUNCTIONALS

In this section we derive the FMF for our model system, i.e. a fluid of CR. We do it in two steps. First, the 2D functional for HD of radius R is projected on the external surface of a cylinder of radius R_0 , providing a 1D functional for a fluid of CA (Section II A). Then, this 1D functional is developed along the orthogonal dimension to obtain a 2D functional for the CR fluid (Section II B). The two cases $R_0 < R$ and $R_0 > R$ are discussed separately in each case, since they give rise to fundamentally different expressions. In the last part of this section the resulting functionals are shown to be dimensionally consistent.

A. Functional for CA

We start from the FMF excess free energy for a fluid of HD derived in Refs. [16, 18], i.e.

$$\beta\mathcal{F}_{\text{ex}}^{(\text{HD})}[\rho] = \int d\mathbf{r} \Phi_{2\text{D}}^{(\text{HD})}(\mathbf{r}), \quad (1)$$

where $\mathbf{r} = (r, \phi)$ is the radius vector in polar coordinates. The reduced free-energy density is defined as

$$\Phi_{2\text{D}}^{(\text{HD})}(\mathbf{r}) = -n_0^{(\text{HD})}(\mathbf{r}) \ln [1 - \eta_{\text{HD}}(\mathbf{r})] + \frac{N_{\text{HD}}(\mathbf{r})}{1 - \eta_{\text{HD}}(\mathbf{r})}, \quad (2)$$

where the weighted densities are convolutions of the two-dimensional density profile $\rho_{2\text{D}}(\mathbf{r})$:

$$n_0^{(\text{HD})}(\mathbf{r}) = \frac{1}{2\pi R} \int d\mathbf{r}_1 \rho_{2\text{D}}(\mathbf{r}_1) \delta(R - |\mathbf{r} - \mathbf{r}_1|), \quad (3)$$

$$\eta_{\text{HD}}(\mathbf{r}) = \int d\mathbf{r}_1 \rho_{2\text{D}}(\mathbf{r}_1) \Theta(R - |\mathbf{r} - \mathbf{r}_1|), \quad (4)$$

$$N_{\text{HD}}(\mathbf{r}) = \frac{1}{(2\pi R)^2} \int d\mathbf{r}_1 \int d\mathbf{r}_2 \rho_{2\text{D}}(\mathbf{r}_1) \rho_{2\text{D}}(\mathbf{r}_2) \mathcal{K}(r_{12}) \delta(R - |\mathbf{r} - \mathbf{r}_1|) \delta(R - |\mathbf{r} - \mathbf{r}_2|), \quad (5)$$

with $\delta(x)$ and $\Theta(x)$ the Dirac-delta and Heaviside functions, respectively. Note that $\eta_{\text{HD}}(\mathbf{r})$ is just the local packing fraction, while $N_{\text{HD}}(\mathbf{r})$ is a two-body weighted density defined through the kernel

$$\mathcal{K}(r) = 4\pi R^2 x \sin^{-1}(x) \sqrt{1 - x^2} \Theta(1 - x), \quad x \equiv \frac{r}{2R}. \quad (6)$$

We now restrict the degrees of freedom by imposing that the HD centers of mass be located on a circumference of radius R_0 :

$$\rho_{2\text{D}}(r, \phi) = \rho_{1\text{D}}(\phi) \delta(R_0 - r), \quad (7)$$

where $\rho_{1\text{D}}(\phi)$ is the 1D density profile, and substitute Eq. (7) into Eqs. (3), (4) and (5). Then we take the following steps (details of which can be found in Appendix A): (i) A first change of variables $(\phi_i, r_i) \rightarrow (\phi_i, \xi_i)$, $i = 1, 2$, with $\xi_i = |\mathbf{r} - R_0 \mathbf{u}_i|$ [$\mathbf{u}_i = (\cos \phi_i, \sin \phi_i)$ are unit vectors] to evaluate the weighted densities. As a result they become functions solely of ϕ and r . (ii) Express the weighted densities as a function of the three angles $\alpha(r)$, $\theta(r)$ and

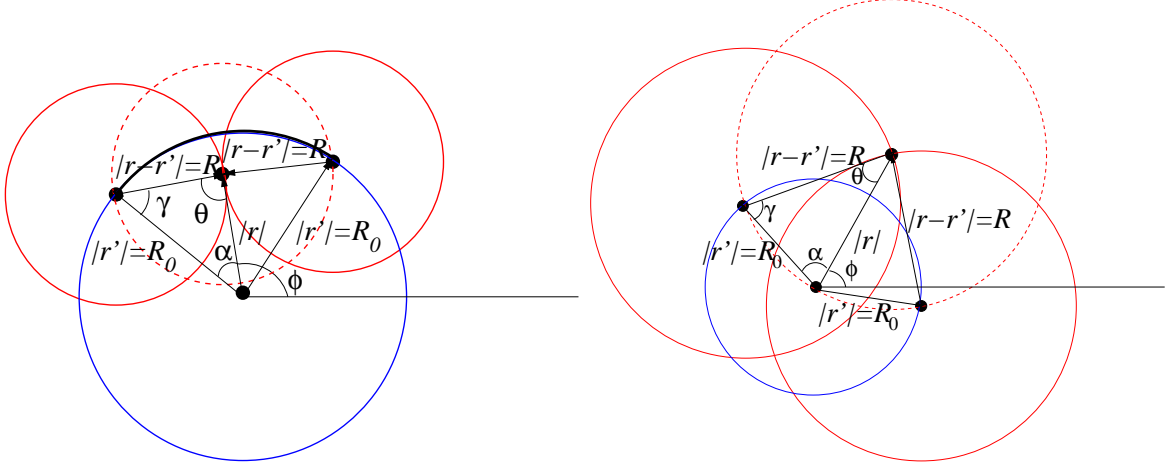


FIG. 1: (Color online) Sketch of the HDs configuration on a circle with $R_0 > R$ (left) and $R_0 < R$ (right).

$\gamma(r)$ [the inner angles of the triangle of sides r , R and R_0 , see Fig. 1] and of their derivatives with respect to r . (iii) Write the second term of the expression for the free-energy density (2) as a sum of the derivatives of the first term with respect to α and ϕ . (iv) A second change of variables $(\phi, r) \rightarrow (\phi, \gamma)$ in Eq. (1). (v) Use of the periodicity of the density profile with respect to the azimuthal angle, $\rho(r, \phi) = \rho(r, \phi + 2\pi)$, and integration by parts to finally arrive at the following expression for the excess part of the DF of HD:

$$\beta \mathcal{F}_{\text{ex}}^{(\text{HD})}[\rho] = \frac{R_0}{\pi} \int_0^{2\pi} d\phi \int_0^\pi d\gamma \left\{ \Psi(\phi, \alpha(\gamma)) + \frac{\partial \Psi}{\partial \alpha}(\phi, \alpha(\gamma)) \theta^*(\gamma) \left| \frac{d\alpha}{d\gamma}(\gamma) \right| \right\}. \quad (8)$$

Here the shorthand notations $\Psi(\phi, \alpha) = -n_{0+}(\phi, \alpha) \ln[1 - \eta_{\text{HD}}(\phi, \alpha)]$ and $n_{0+}(\phi, \alpha) = [\rho_{1\text{D}}(\phi + \alpha) + \rho_{1\text{D}}(\phi - \alpha)]/2$ were used, while the local packing fraction and the angle θ^* are defined as $\eta_{\text{HD}}(\phi, \alpha) = R_0 \int_{\phi-\alpha}^{\phi+\alpha} d\phi_1 \rho_{1\text{D}}(\phi_1)$ and $\theta^* = \theta$ if $0 \leq \theta \leq \pi/2$, while $\theta^* = \pi/2 - \theta$ if $\pi/2 < \theta \leq \pi$.

1. The case $R_0 > R$

A look at Fig. 1 allows us to write the following two relations between the angles α and γ :

$$\frac{d\alpha}{d\gamma} \geq 0 \quad \text{if} \quad 0 < \gamma \leq \gamma_0, \quad \frac{d\alpha}{d\gamma} < 0 \quad \text{if} \quad \gamma_0 < \gamma \leq \pi, \quad (9)$$

where $\gamma_0 = \cos^{-1}(R/R_0)$, $\theta_0 \equiv \theta(\gamma_0) = \pi/2$ and $\alpha_0 \equiv \alpha(\gamma_0) = \sin^{-1}(R/R_0)$. After some lengthy calculations, which can be followed in detail in Appendix A 1, we obtain from (8)

and (9) the following dimensional cross-over:

$$\beta\mathcal{F}_{\text{ex}}^{(\text{HD})}[\rho] \rightarrow \beta\mathcal{F}_{\text{ex}}^{(\text{CA})}[\rho] = R_0 \int_0^{2\pi} d\phi \Phi_{1\text{D}}^{(\text{CA})}(\phi), \quad (10)$$

with $\Phi_{1\text{D}}^{(\text{CA})}(\phi)$ the 1D Percus free-energy density:

$$\Phi_{1\text{D}}^{(\text{CA})}(\phi) \equiv \Psi(\phi, \alpha_0) = -n_0^{(\text{CA})}(\phi) \ln[1 - \eta_{\text{CA}}(\phi)], \quad (11)$$

and with the corresponding weighted densities

$$n_0^{(\text{CA})}(\phi) = n_{0+}(\phi, \alpha_0) = \frac{1}{2} [\rho_{1\text{D}}(\phi - \alpha_0) + \rho_{1\text{D}}(\phi + \alpha_0)], \quad (12)$$

$$\eta_{\text{CA}}(\phi) = \eta_{\text{HD}}(\phi, \alpha_0) = R_0 \int_{\phi - \alpha_0}^{\phi + \alpha_0} d\phi' \rho_{1\text{D}}(\phi'). \quad (13)$$

Here the index ‘CA’ means that these densities are evaluated on a circular arc of length $2R_0\alpha_0$. Then we have proved that the excess part of the HD free-energy functional reduces to that of hard CA.

2. The case $R_0 < R$

In this case we always have

$$\frac{d\alpha}{d\gamma} < 0, \quad \forall \gamma, \quad 0 \leq \theta < \pi/2 \quad (14)$$

(see Fig. 1). After some algebra (described in detail in Appendix A 2), we obtain from (8) and (14) the following dimensional cross-over:

$$\beta\mathcal{F}_{\text{ex}}^{(\text{HD})}[\rho] \rightarrow \beta\mathcal{F}_{\text{ex}}^{(\text{CA})}[\rho] = \eta_{\text{CA}} + (1 - \eta_{\text{CA}}) \ln(1 - \eta_{\text{CA}}), \quad (15)$$

corresponding to the exact 0D functional of CA (such that at most one arc can exist on the circle). The mean number of particles is

$$\eta_{\text{CA}} \equiv R_0 \int_{-\pi}^{\pi} d\phi' \rho_{1\text{D}}(\phi') = 2\pi R_0 \bar{\rho}_{1\text{D}}, \quad (16)$$

with $\bar{\rho}_{1\text{D}}$ the mean number density over the circle of radius R_0 .

B. Functional for CR

We now define a collection of CR, each consisting of two parallel curved edges formed by circular arcs of length $2R_0\alpha_0$ and two parallel straight lines of length L perpendicular to the former. The centers of mass of the CR are located on a 2D cylindrical surface of radius R_0 . The density profile will be $\rho_{2D}(\phi, z)$, where z is the coordinate along the cylinder axis and ϕ is the azimuthal angle. The functional for this model will be obtained in the two cases.

1. The case $R_0 > R$

First, we define the local packing fraction as

$$\eta_{\text{CR}}(\phi, z) = R_0 \int_{\phi-\alpha_0}^{\phi+\alpha_0} d\phi' \int_{z-L/2}^{z+L/2} dz' \rho_{2D}(\phi', z'), \quad (17)$$

and the weighted density

$$n_{1,\perp}^{(\text{CR})}(\phi, z) = \frac{1}{2} \int_{z-L/2}^{z+L/2} dz' [\rho_{2D}(\phi - \alpha_0, z') + \rho_{2D}(\phi + \alpha_0, z')]. \quad (18)$$

Let us write the modified 1D Percus free-energy density:

$$\tilde{\Phi}_{1D}(\phi, z) = -n_{1,\perp}^{(\text{CR})}(\phi, z) \ln [1 - \eta_{\text{CR}}(\phi, z)]. \quad (19)$$

Note that this is in fact a local free-energy density corresponding to the CA fluid. Now the CR free-energy density can be calculated by applying a differential operator $\partial/\partial L$ to the modified 1D free-energy density [17]:

$$\Phi_{2D}^{(\text{CR})}(\phi, z) = \frac{\partial}{\partial L} \tilde{\Phi}_{1D}(\phi, z), \quad (20)$$

which results in

$$\Phi_{2D}^{(\text{CR})}(\phi, z) = -n_0^{(\text{CR})}(\phi, z) \ln [1 - \eta_{\text{CR}}(\phi, z)] + \frac{n_{1,\perp}^{(\text{CR})}(\phi, z) n_{1,\parallel}^{(\text{CR})}(\phi, z)}{1 - \eta_{\text{CR}}(\phi, z)}, \quad (21)$$

where we have defined

$$n_0^{(\text{CR})}(\phi, z) = \frac{\partial}{\partial L} \tilde{n}_{1,\perp}^{(\text{CR})}(\phi, z) = \frac{1}{4} [\rho_{2D}(\phi_-, z_-) + \rho_{2D}(\phi_-, z_+) + \rho_{2D}(\phi_+, z_-) + \rho_{2D}(\phi_+, z_+)], \quad (22)$$

$$n_{1,\parallel}^{(\text{CR})}(\phi, z) = \frac{\partial}{\partial L} \eta_{\text{CR}}(\phi, z) = \frac{R_0}{2} \int_{\phi_-}^{\phi_+} d\phi' [\rho_{2D}(\phi', z_-) + \rho_{2D}(\phi', z_+)], \quad (23)$$

and $z_{\pm} = z \pm L/2$, $\phi_{\pm} = \phi \pm \alpha_0$. Then the excess CR free-energy functional can be calculated as

$$\beta \mathcal{F}_{\text{ex}}^{(\text{CR})}[\rho] = R_0 \int_0^{2\pi} d\phi \int_{-\infty}^{\infty} dz \Phi_{2\text{D}}^{(\text{CR})}(\phi, z). \quad (24)$$

Note that (21) is just the excess free-energy density of a fluid of parallel hard rectangles (PHR) of length L and width $\sigma = 2R_0\alpha_0$ which in turn coincides with that of the parallel hard squares (PHS) fluid after scaling one of the edge-lengths [17]. Also note that, taking the limit $R_0/R \rightarrow \infty$, changing the variable ϕ to $x \equiv R_0\phi$ and setting $\sigma = 2R_0\alpha_0$, we obtain from (24) the excess part of the density functional of PHR on a flat surface of edge-lengths σ and L given in Ref. [17]. Thus the present functional has the same degree of exactness as that for the PHS fluid. As was shown in [20], the minimization of the latter gives a phase behavior in which the columnar and crystalline phases both bifurcate from the uniform fluid branch at $\eta \approx 0.54$, with the columnar phase being the stable phase (although the difference between free energies is very small) up to $\eta \approx 0.73$, where a weak first-order columnar-to-crystal transition occurs. Single-speed Molecular Dynamics simulations of PHS show a second order melting transition at $\eta \approx 0.79$ [21] similar to the above given value. However, columnar ordering was not found in the simulations.

2. The case $R_0 < R$

If $R_0 < R$ we define a 1D local packing fraction as

$$\eta_{\text{CR}}(z) = R_0 \int_{-\pi}^{\pi} d\phi \int_{z-L/2}^{z+L/2} dz' \rho_{2\text{D}}(\phi', z'), \quad (25)$$

and a modified 0D free-energy density as

$$\tilde{\Phi}_{0\text{D}}^{(\text{CR})}(z) = \eta_{\text{CR}}(z) + [1 - \eta_{\text{CR}}(z)] \ln [1 - \eta_{\text{CR}}(z)]. \quad (26)$$

The CR free-energy density for this case can be obtained by using the differential operator $\partial/\partial L$ applied to the modified 0D free-energy density [17]:

$$\frac{\partial}{\partial L} \tilde{\Phi}_{0\text{D}}^{(\text{CR})}(z) = R_0 \Phi_{1\text{D}}^{(\text{CR})}(z) = -R_0 n_0^{(\text{CR})}(z) \ln [1 - \eta_{\text{CR}}(z)], \quad (27)$$

where

$$n_0^{(\text{CR})}(z) = R_0^{-1} \frac{\partial}{\partial L} \eta_{\text{CR}}(z) = \frac{1}{2} \int_{-\pi}^{\pi} d\phi' [\rho_{2\text{D}}(\phi', z_-) + \rho_{2\text{D}}(\phi', z_+)]. \quad (28)$$

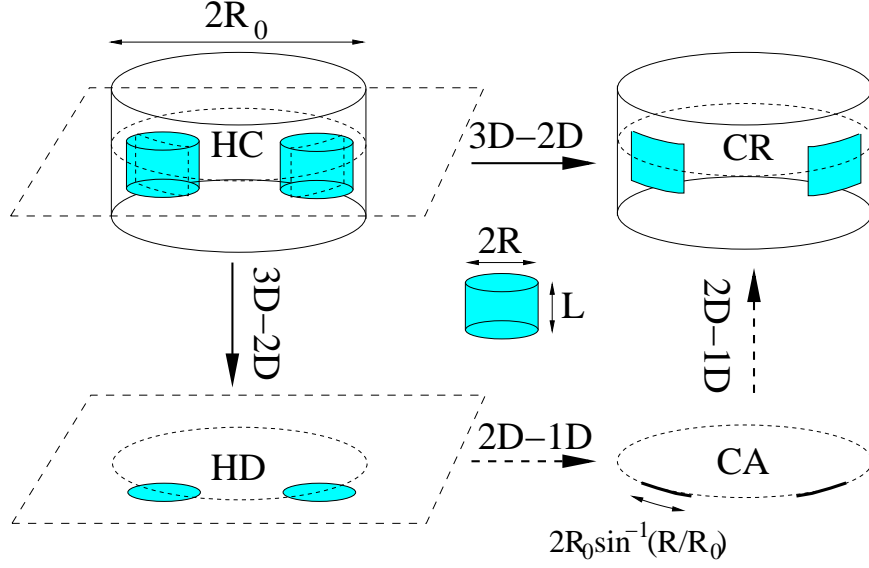


FIG. 2: (Color online) Dimensional cross-over of HC of radius R and length L confined on a cylindrical surface of radius R_0 . This $3D \rightarrow 2D$ crossover becomes HC into CR. Also shown is the $3D \rightarrow 2D$ cross-over when the HC are confined on a flat surface. This cross-over becomes HC into HD. Finally the $2D \rightarrow 1D$ cross-over from HD or CR when both are confined on a circumference of radius R_0 results in CA of length $2R_0 \sin^{-1}(R/R_0)$ (the arc of closest approach between two HD). Dashed arrows indicate the route to obtain the FMF for CR.

The excess free-energy functional is now

$$\beta \mathcal{F}_{\text{ex}}^{(\text{CR})}[\rho] = 2\pi R_0 \int_{-\infty}^{\infty} dz \Phi_{1D}^{(\text{CR})}(z). \quad (29)$$

C. Confined hard cylinders

The free energy of a collection of CR can be obtained from two different routes. In the previous two sections we used a two-step process: first, the HD fluid was projected on the circumference of a circle, giving the functional for CA. This in turn was developed along z to give the free energy for CR. There is another possible route which starts from the 3D functional for hard cylinders (HC). The HC excess free-energy is

$$\beta \mathcal{F}_{\text{ex}}^{(\text{HC})}[\rho] = \int dz \int d\phi \int dr r \Phi_{3D}^{(\text{HC})}(r, \phi, z), \quad (30)$$

with $\Phi_{3D}^{(\text{HC})}(r, \phi, z)$ the excess free-energy density [18, 22]. Now we confine the HC on a plane perpendicular to the cylinder axes at $z = 0$ by choosing the 3D density profile $\rho_{3d}(r, \phi, z) =$

$\rho_{2d}(r, \phi)\delta(z)$. Inserting this into (30), we obtain an excess free-energy

$$\beta\mathcal{F}_{\text{ex}}^{(\text{HD})}[\rho] = \int d\phi \int dr r \Phi_{2D}^{(\text{HD})}(r, \phi), \quad (31)$$

where, due to the dimensional crossover consistency, $\Phi_{2D}^{(\text{HD})}(r, \phi)$ is given by Eq. (2), i.e. coincides with the HD free-energy density. Selecting now $\rho(r, \phi, z) = \rho(\phi, z)\delta(R_0 - r)$ (i.e. confining the HC on a 2D cylindrical surface of radius R_0) and inserting it into Eq. (30), we obtain, for $R_0 > R$

$$\beta\mathcal{F}_{\text{ex}}^{(\text{CR})}[\rho] = R_0 \int_0^{2\pi} d\phi \int_{-\infty}^{\infty} dz \Phi_{2D}^{(\text{CR})}(\phi, z), \quad (32)$$

where $\Phi_{2D}^{(\text{CR})}(\phi, z)$ is the free-energy density of curved rectangles (20). When $R_0 < R$ we obtain

$$\beta\mathcal{F}_{\text{ex}}^{(\text{CR})}[\rho] = 2\pi R_0 \int_{-\infty}^{\infty} dz \Phi_{1D}^{(\text{CR})}(z), \quad (33)$$

where $\Phi_{1D}^{(\text{CR})}(z)$ is the free-energy density (27).

We sketch in Fig. 2 the dimensional cross-overs involved in the preceding discussion.

III. PHASE BEHAVIOUR OF CR

In this section we analyze the phase behaviour of the CR fluid predicted by the functional derived in the previous section, in the non-trivial case $R_0 > R$. We start by presenting the numerical treatment in Section III A and then show the results in Section IV.

A. Minimization technique

The total free-energy density functional (ideal plus excess parts) per unit of area is

$$\frac{\beta\mathcal{F}^{(\text{CR})}[\rho]}{2\pi R_0 \mathcal{L}} = \frac{1}{2\pi d} \int_0^{2\pi} d\phi \int_0^d dz \left[\Phi_{\text{id}}^{(\text{CR})}(\phi, z) + \Phi_{2D}^{(\text{CR})}(\phi, z) \right], \quad (34)$$

where \mathcal{L} is the system length along z and

$$\Phi_{\text{id}}^{(\text{CR})}(\phi, z) = \rho_{2D}(\phi, z) [\log \rho_{2D}(\phi, z) - 1], \quad (35)$$

is the ideal part. The excess contribution is given by Eq. (21). The possible ordered phases in the system are smectic (S), columnar (C) and crystal (K) (sketched in Fig. 3).

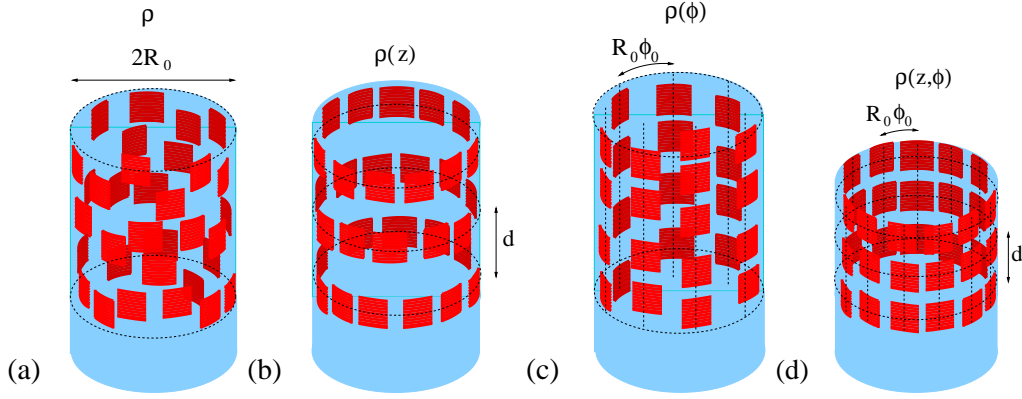


FIG. 3: (Color online) Phases of CR on a cylindrical surface of radius R_0 : (a) N, (b) S, (c) C and (d) K. The lattice parameters and the variables of which the density profiles depend are correspondingly labelled.

A general density profile will be periodic in z (with period d) and ϕ (with period 2π), i.e. $\rho_{2d}(\phi + 2\pi, z + d) = \rho_{2d}(\phi, z)$, and a convenient representation is a double Fourier expansion

$$\rho_{2d}(\phi, z) = \rho_0 \left[1 + \sum_{(k,m) \neq (0,0)} s_{km} \cos(kN_0\phi) \cos(qmz) \right], \quad (36)$$

where ρ_0 is the mean density $\rho_0 = (2\pi d)^{-1} \int_0^{2\pi} d\phi \int_0^d dz \rho_{2d}(z, \phi)$, $\{s_{km}\}$ are the Fourier amplitudes, and $q = 2\pi/d$ is the wave-vector along z . Note that $s_{km} = 0 \forall k \neq 0$ corresponds to the S phase, while $s_{km} = 0 \forall m \neq 0$ implies a C phase. In the latter phase the obvious periodicity $\rho_{2d}(\phi) = \rho(\phi + 2\pi)$ must be supplemented with a periodicity $\rho_{2d}(\phi + \phi_0) = \rho_{2d}(\phi)$, with $\phi_0 = 2\pi/N_0$ the period; here the average position of the columns would be located on the vertices of a N_0 -sided regular polygon. N_0 is an integer in the interval $2 - [\pi/\alpha_0]$, with $[x]$ the integer part of x , and $\alpha_0 = \sin^{-1}(R/R_0)$. As an example, if $R_0 = 2R$ we have $N_0^{(\max)} = 6$, a value that can be reached only at close-packing.

Using the above Fourier expansion, the weighted densities (17), (18) and (22), (23) can be calculated from the expressions given in Appendix B [see Eqs. (B2-B4)]. The strategy followed to minimise the functional (34) was to use a truncated Fourier expansion in terms of the amplitudes $\{s_{km}\}$ for $0 \leq k, m \leq M$ (with M selected in such a way as to guarantee an adequate description of the density profile) and then minimise with respect to these amplitudes and the period d . We used a conjugate-gradient method to numerically implement the minimization. All the integrals were calculated using Legendre quadratures with as many roots as necessary to guarantee numerical errors in the amplitudes below 10^{-7} .

As shown in the next section, the unstable or metastable character of the crystalline phase is difficult to obtain by direct minimisation, so in this case we chose to parameterise the density profile as a sum of Gaussians:

$$\begin{aligned}\rho_{2D}(\phi, z) &= (1 - \nu)\zeta_{0\perp}(\phi)\zeta_{0\parallel}(z), \\ \zeta_{0\perp}(\phi) &= \left(\frac{\Lambda_{\perp}}{\pi}\right)^{1/2} \sum_k \exp[-\Lambda_{\perp}R_0^2(\phi - k\phi_0)^2], \\ \zeta_{0\parallel}(z) &= \left(\frac{\Lambda_{\parallel}}{\pi}\right)^{1/2} \sum_k \exp[-\Lambda_{\parallel}(z - kd)^2],\end{aligned}\tag{37}$$

where $\Lambda_{\perp}(2R_0\alpha_0)^2 = \Lambda_{\parallel}L^2 = \Lambda$ is the scaled Gaussian parameter and ν the fraction of vacancies. Within this approximation, the total free energy per unit of area, in reduced units, can be computed from the expression given in Appendix B [see Eq. (B5)]. We minimized (B5) with respect to Λ and ν . The mean packing fraction can be computed as $\eta_0 = \frac{(1 - \nu)a}{R_0\phi_0d}$ (with $a = 2R_0\alpha_0L$ the particle area) and thus for fixed η_0 and ν we can compute the period d from the latter equation. The integrals of Eq. (B5) were evaluated using a Gauss-Hermite quadrature while the minimization was carried out using the Newton-Raphson method with supplied numerical derivatives.

IV. RESULTS

We minimized (34) using the Fourier expansion of the density profile (36) for the S and C phases and for four different values of $R_0/R = 1.04, 1.30, 1.66$ and 2.00 . The results are shown in Fig. 4 (a) in which we plot the difference between the free-energies per unit area corresponding to the C and S phases i.e. $\Delta\Phi_C^* = \Phi_C^* - \Phi_S^*$ (with $\Phi^* = \frac{\beta\mathcal{F}[\rho_{eq}]a}{2\pi R_0\mathcal{L}}$), as a function of the mean packing fraction η_0 . For the C phase the number of columns for each value of R_0/R are $N_0 = 2, 3, 4$ and 5 , respectively. As can be seen, $\Delta\Phi_C^* \geq 0$ always, implying that the S phase is the most stable phase. This behavior can be understood if we take into account that the C period in reduced units is $\phi_0^* = \phi_0R_0/(2\alpha_0R_0) = \pi/(N_0\alpha_0)$ which in turn is different from that of PHR (remember that the excess part of the free-energy density of CR can be obtained from that of PHR by the mapping $\sigma \rightarrow 2\alpha_0R_0$, with σ the width of the rectangle); the latter is calculated by minimizing the free-energy with respect to the period. Note that, for PHR, the C and S phases have the same free energies (the

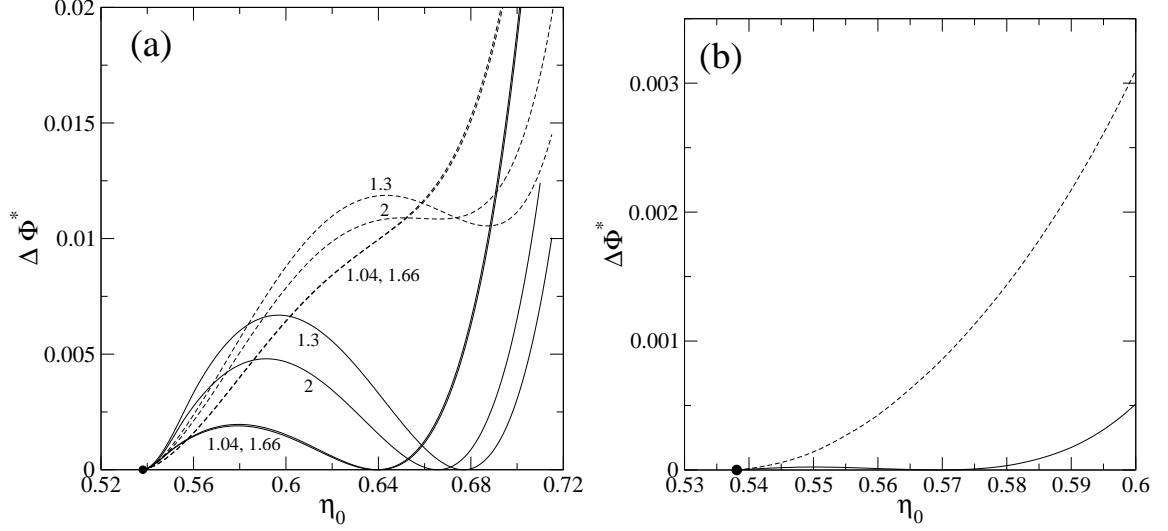


FIG. 4: (a): Free-energy differences $\Delta\Phi_{C,K}^*$ (see the text for the definition) between the C and S (solid lines) phases and K and S phases (dashed lines) and for different values of R_0/R , in (a) they are equal to 1.04, 1.3, 1.66 and 2. Different lines are labelled with their corresponding values of R_0/R . The number of columns N_0 in the C phases are 2, 3, 4 and 5, respectively. In (b) $R_0/R = 1.05$ and $N_0 = 2$. The crystalline phase in (b) was calculated through the free-energy minimization with respect to the Fourier amplitudes of the density-profile Fourier expansion.

PHR can be obtained by scaling the PHS along one direction). However in the present case the value of ϕ_0^* is imposed once we fix R_0/R and the number of columns N_0 , the latter being dictated by the commensuration of a CA of length $2\alpha_0 R_0$ in a circle of perimeter $2\pi R_0$, i.e. $2 \leq N_0 \leq [\pi/\alpha_0]$. In a case when different values of N_0 are possible, we select the one which minimizes the free energy. It is interesting to note that $\Delta\Phi^* = 0$ both at the bifurcation point η_0^* and at that value of η_0 for which the periods in reduced units of CR (ϕ_0^*) and of hard parallel rectangles (HPR) on a plane ($d_{\text{HPR}}^* \equiv d_{\text{HPR}}/\sigma$) are exactly the same. Finally, from Fig. 4(a), we can see that $\Delta\Phi_c^*$ for the cases $R_0/R = 1.04$ ($N_0 = 2$) and 1.66 ($N_0 = 4$) are indistinguishable from each other. The reason behind this behavior is that the commensuration numbers $\pi/(N_0\alpha_0)$ [ratio between the perimeter of the circle ($2\pi R_0$) and the total length of the N_0 arcs of length $2R_0\alpha_0$] are approximately equal in both cases (1.2153 and 1.2148, respectively).

In the same figure we also plot $\Delta\Phi_K^* = \Phi_K^* - \Phi_S^*$, i.e. the difference between the free energies per unit volume of the K and S phases. For this case we have used the Gaussian

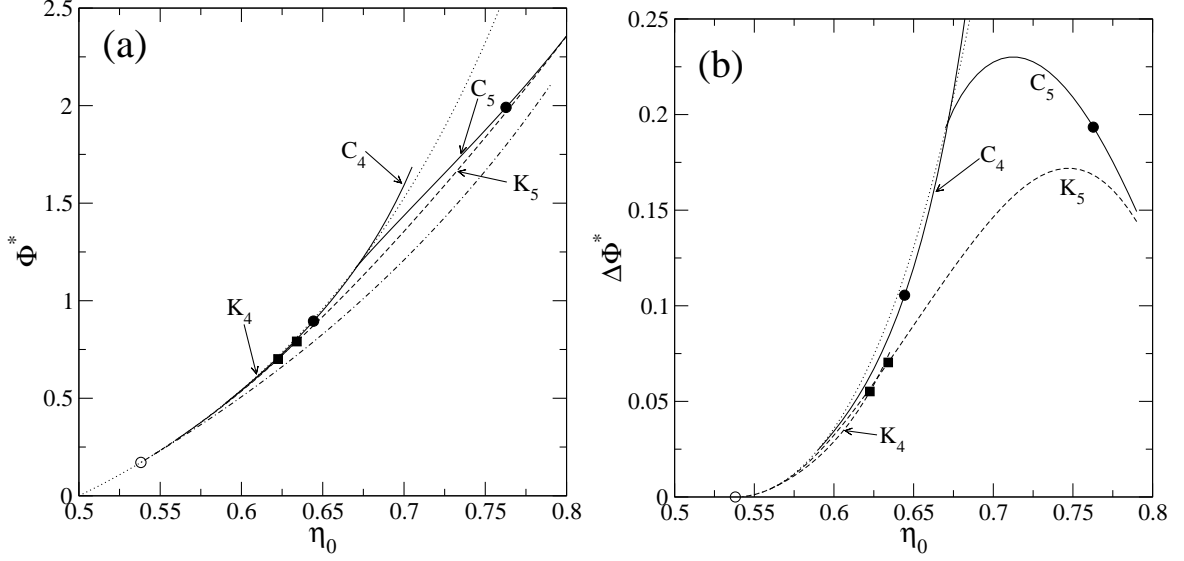


FIG. 5: (a): Free energies per unit of area (we plot $\Phi^* + \eta_0 \ln(a)$) of N (dotted), S (dot-dashed), C₄ and C₅ (solid lines correspondingly labelled), K₄ and K₅ (dashed lines correspondingly labelled) phases as a function of η_0 for $R_0/R = 1.8$. The open circle indicates the N-S bifurcation point. Circles indicate the metastable C₄-C₅ coexistence, while squares correspond to the metastable K₄-K₅ coexistence. (b): Free-energy density differences between the S and all the phases shown in (a). The lines and symbols have the same meaning as in (a).

parametrization (37) and minimized (B5) with respect to Λ and d^* [we tried to use the Fourier expansion (36) with K symmetry, but the numerical algorithm converged to a solution with C or S symmetry always, except for those values of η_0 close enough to the bifurcation point, an example of which is shown in Fig. 4 (b)]. In Fig. 4 (a) we see that the K phase has a larger free energy compared to the S phase. However now $\Delta\Phi_K^*$ does not touch the η_0 -axis tangentially, because the PHR free energies corresponding to the C (or S) and K phases are not equal, the former being energetically favored up to $\eta_0 \sim 0.73$ [20].

It is interesting to note that the N-S transition exists even for values of $R_0/R \gtrsim 1$. As already shown, for $R_0/R < 1$ this transition is absent since the free energy functional is in fact the 1D functional for hard rods (Percus functional).

Now we present the results for $R_0/R = 1.8$, a value for which the free-energy branches of the C phases with $N_0 = 4$ (C₄) and 5 (C₅) columns intersect at some value of η_0 . These free energies are plotted in Fig. 5. The C₄ and C₅ branches are above those of the K_{4,5} and S phases. This result could change in a confined binary fluid of HC with different lengths. For

dissimilar enough lengths, the S and K phases would be energetically unfavored with respect to the C_{N_0} phases. In this situation a C_4 - C_5 transition could take place as η_0 increases. For some higher values of R_0/R we will find a cascade of $C_{N_0-1} \rightarrow C_{N_0}$ transitions for different values of N_0 because multiple values of N_0 fulfills the constraint $2 \leq N_0 \leq [\pi/\alpha_0]$.

Finally, we have calculated all the energy branches of stable or metastable phases for $R_0/R = 4$, which are plotted in Fig. 6. For this case there are two columnar, C_{10} and C_{11} , and two crystalline, K_{10} and K_{11} , phases which are metastable with respect to the Sm phase (except the K_{11} phase, which is stable in a small range of η_0). We show in Fig. 6 the metastable C_{10} - C_{11} and K_{10} - K_{11} coexistences, using different symbols. Note that the coexistence gaps decrease with respect to the case $R_0/R = 1.8$, a trend that should be confirmed if the value R_0/R were to be increased even more. It is interesting to note that there is a relatively small interval of packing fractions (dashed region in the figure) where the K_{11} phase becomes reentrant. This interval should increase for higher values of R_0/R and in fact, in the limit $R_0/R \rightarrow \infty$ (the HPR limit), the K phase becomes stable for $\eta \gtrsim 0.73$ [20].

V. DENSITY FUNCTIONAL OF SPHERICAL LENSES

In principle the same dimensional cross-over procedure can be implemented on the density functional for HS of radii R whose centers of mass are restricted to be on a spherical surface of radius R_0 . If the density functional for HS adequately fulfills the dimensional cross-over property, the resulting functional, that of a fluid consisting of hard spherical lenses (SL) [obtained from the intersection between the spherical surface and a cone with vertex at the origin and with solid angle equal to $4\pi \sin^2(\alpha_0/2) = 2\pi [1 - \sqrt{1 - (R/R_0)^2}]$], should coincide, when $R_0/R > 1$, with the 2D functional for HD [Eq. (2)] where the density profile this time is a periodic function of the spherical angles $\rho(\phi, \theta) = \rho(\phi + 2\pi, \theta + 2\pi)$ and the semi-length of the SL is equal to $R_0\alpha_0 = R_0 \sin^{-1}(R/R_0)$. We present in Appendix C the explicit expressions for the weighted densities of SL. With the present tool, the study of the freezing of HS on a spherical surface could be carried out. An interesting point to be studied is how the symmetry of the crystalline structure, and the presence of defects and vacancies, could change with the ratio R_0/R .

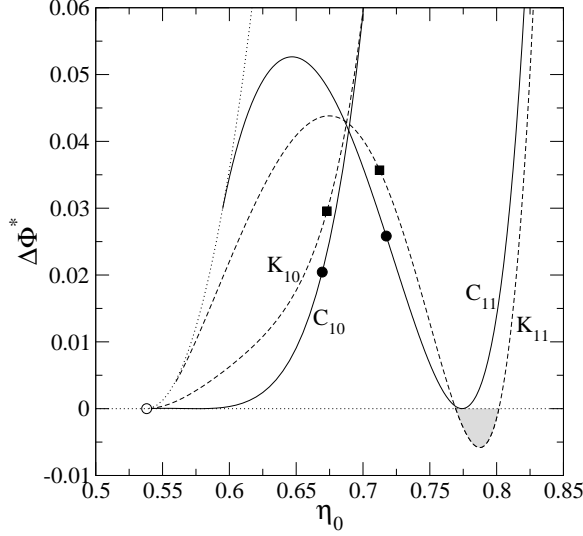


FIG. 6: Free-energy density differences between the S and the N (dotted), C_{10} and C_{11} (solid lines correspondingly labelled), K_{10} and K_{11} (dashed lines correspondingly labelled) phases as a function of the mean packing fraction η_0 for $R_0/R = 4$. The open circle indicates the N-S bifurcation point. The circles and squares show the C_{10} - C_{11} and K_{10} - K_{11} metastable coexistences, respectively. The grey region shows the packing fraction interval in which the K_{11} has a lower free energy than the S phase.

VI. CONCLUSIONS

The present work followed two motivations. The first was to illustrate the dimensional cross-over criterion as a powerful projection tool to obtain a DF for hard particles with centres of mass constrained to be on a particular (in the present case cylindrical) surface from a given DF which fulfills this criterion. The second motivation was the study of the phase behaviour of CR (the particles obtained by projecting the centres of mass of HC onto a cylindrical surface). We show that surface curvature has a profound impact on the stability of the liquid-crystal phases of curved rectangles as compared with the planar case. The projection method is quite general and can be used to obtain DFs for other particle geometries and other surfaces. As an example, we proposed in Sec. V a DF for spherical lenses, i.e. the particles obtained when the centres of mass of HS are placed on an external spherical surface.

During the derivation of DF for CR we proved the dimensional cross-over properties of the FMF of HD of radii R when their centers of mass are constrained to be on a circumference

of radius R_0 . Depending on the ratio R_0/R the original 2D density functional reduces to the 1D Percus functional (when $R_0/R > 1$) or to the 0D functional ($R_0/R < 1$), which are both exact limits. From these dimensionally-reduced functionals, using the dimensional expansion procedure, we derive the density functional for CR moving on a cylindrical surface of radius R_0 . We show that this functional is equivalent to that of PHR on a flat surface with the edge-lengths of the particles being $\sigma = 2R_0 \sin^{-1}(R/R_0)$ and L . We minimized the functional for CR to get the phase behavior for different values of R_0/R . When $R_0/R > 1$ we obtain that the most stable phase is S, as compared to the C or K phases, except for some relatively large values of R_0/R and small density intervals in which we find a reentrant K phase. We find also metastable C_{n-1} - C_n or K_{n-1} - K_n transitions related to the commensuration between the particle width and the perimeter of the cylindrical surface. These transitions could become stable when the confined HC have different lengths (it is well known that the length polydispersity destroy the S ordering). When $R_0/R < 1$ the density functional of CR coincides with the 1D Percus functional, so that the system does not exhibit any phase transition. We are presently performing MC simulations of CR with the aim to compare the phase behavior with that obtained from the present FMF. Note that the latter, being a 2D functional, is not exact.

The present phase behavior points to possible textures that adsorbed molecules (for example proteins) on cylindrical membranes could exhibit. If these molecules are highly anisotropic, highly oriented along the cylinder axis and interact repulsively with each other, their stable textures should include only nematic and smectic-like configurations for low and high densities, respectively.

The wall of some rod-shaped bacteria grows in the direction of the cylinder axis, keeping the radius approximately constant. The new proteins come from the inside of the cell to the wall. In Ref. [23] the authors explain cell growth by the insertion of these proteins into the wall and their subsequent active diffusion along the perimeter of the cylinder via a dislocation-mediated growth. The model assumes that the proteins form a square lattice on a surface of the cylinder (this is apparently confirmed by experiments). Protein diffusion along the wall-perimeter (activated by the cell machinery) departs from some of these dislocations which constitute the source of the new proteins coming from the cell. Our results show that the smectic-like configuration of proteins favors their transversal diffusion. Also the sources of new molecules could be located at any position inside the smectic layers with marginal

energy cost associated to the spatial deformation of layers (as they are fluid-like). However this mechanism makes the cylindrical membrane grow in the transversal direction. Growth along the longitudinal direction is possible by creating new smectic layers and consequently smectic-like defects in the layers. This is an alternative mechanism that might explain the growth of cells whose membranes are constituted by molecules that form smectic-like textures.

Appendix A: $2D \rightarrow 1D, 0D$ dimensional cross-over of HD on a circle

Substitution of (7) into Eq. (3) gives

$$n_0^{(\text{HD})}(\mathbf{r}) = \frac{R_0}{2\pi R} \int_0^{2\pi} d\phi_1 \delta(R - |\mathbf{r} - R_0 \mathbf{u}_1|) \rho_{1D}(\phi_1), \quad (\text{A1})$$

where $\mathbf{u}_1 = (\cos \phi_1, \sin \phi_1)$ is a unit vector. Here the polar radius r is restricted to be in the interval $[|R_0 - R|, R_0 + R]$. Using the change of variables $\xi = |\mathbf{r} - R_0 \mathbf{u}_1| = \sqrt{r^2 + R_0^2 - 2rR_0 \cos(\phi - \phi_1)}$, where $\mathbf{r} = r\mathbf{u}$, $\mathbf{u} = (\cos \phi, \sin \phi)$ and $\mathbf{u} \cdot \mathbf{u}_1 = \cos(\phi - \phi_1)$, we obtain

$$n_0^{(\text{HD})}(\mathbf{r}) = \frac{1}{2\pi r} \frac{[\rho_{1D}(\phi + \alpha(r)) + \rho_{1D}(\phi - \alpha(r))]}{\sqrt{1 - \left(\frac{r^2 + R_0^2 - R^2}{2rR_0}\right)^2}} \Theta(R - |r - R_0|), \quad (\text{A2})$$

where

$$\alpha(r) \equiv \cos^{-1} \left(\frac{r^2 + R_0^2 - R^2}{2rR_0} \right) \quad (\text{A3})$$

Now we calculate the two-body weighted density $N_{\text{HD}}(\mathbf{r})$ by substituting $\rho_{2D}(\mathbf{r}_i) = \rho_{1D}(\phi_i) \delta(R_0 - r_i)$ [which is equivalent to setting $\mathbf{r}_i = R_0 \mathbf{u}_i$ with $\mathbf{u}_i = (\cos \phi_i, \sin \phi_i)$] into Eq. (5). Noting that $r_{12} = |\mathbf{r}_1 - \mathbf{r}_2| = 2R_0 |\sin(\phi_{12}/2)|$ and using Eq. (6), we obtain

$$\mathcal{K}(r_{12}) = 4\pi R^2 \frac{R_0}{R} |\sin(\phi_{12}/2)| \sin^{-1} \left(\frac{R_0}{R} |\sin(\phi_{12}/2)| \right) \sqrt{1 - \left(\frac{R_0}{R} \sin(\phi_{12}/2) \right)^2}. \quad (\text{A4})$$

Using again $\xi_i = |\mathbf{r} - \mathbf{r}_i|$, taking into account that $|\sin(\phi_{12}/2)|_{\xi_i=R} = |\sin \alpha(r)|$, and using (5), we obtain

$$\begin{aligned} N_{\text{HD}}(\mathbf{r}) &= \frac{R_0}{\pi r^3} \frac{\rho_{1D}(\phi - \alpha(r)) \rho_{1D}(\phi + \alpha(r))}{\sqrt{1 - \left(\frac{r^2 + R_0^2 - R^2}{2rR_0}\right)^2}} |R^2 + r^2 - R_0^2| \\ &\quad \times \sin^{-1} \left(\frac{R_0}{R} \sqrt{1 - \left(\frac{r^2 + R_0^2 - R^2}{2rR_0}\right)^2} \right) \Theta(R - |r - R_0|). \end{aligned} \quad (\text{A5})$$

The local packing fraction (4) results in

$$\eta_{\text{HD}}(\mathbf{r}) = R_0 \int_0^{2\pi} d\phi_1 \rho_{1\text{D}}(\phi_1) \Theta(R - |\mathbf{r} - R_0 \mathbf{u}_1|) = R_0 \int_{\phi-\alpha(r)}^{\phi+\alpha(r)} d\phi_1 \rho_{1\text{D}}(\phi_1), \quad (\text{A6})$$

where we used the fact that the condition $|\mathbf{r} - R_0 \mathbf{u}_1| \leq R$ implies $|\phi - \phi_1| \leq \alpha(r)$. The weighted densities can be written in terms of the angle $\alpha(r)$ and the new angles $\theta(r)$ and $\gamma(r)$, defined in Fig. 1:

$$n_0^{(\text{HD})}(\mathbf{r}) = \frac{R_0}{2\pi r} [\rho_{1\text{D}}(\phi - \alpha(r)) + \rho_{1\text{D}}(\phi + \alpha(r))] \frac{d\gamma}{dr}(r), \quad (\text{A7})$$

$$N_{\text{HD}}(\mathbf{r}) = \frac{2R_0^2}{\pi r} \rho_{1\text{D}}(\phi - \alpha(r)) \rho_{1\text{D}}(\phi + \alpha(r)) \left| \frac{d\alpha}{d\gamma}(r) \right| \theta^*(r) \frac{d\gamma}{dr}(r), \quad (\text{A8})$$

where

$$\theta^* = \begin{cases} \theta, & \text{if } 0 \leq \theta \leq \pi/2 \\ \pi - \theta, & \text{if } \pi/2 \leq \theta \leq \pi. \end{cases} \quad (\text{A9})$$

The following equation is satisfied:

$$\rho_{1\text{D}}(\phi - \alpha(r)) \rho_{1\text{D}}(\phi + \alpha(r)) = \frac{1}{4} \left\{ \frac{2}{R_0} n_{0+}(\mathbf{r}) \frac{\partial \eta_{\text{HD}}}{\partial \alpha}(\mathbf{r}) - \frac{1}{R_0^2} \left[\frac{\partial \eta_{\text{HD}}}{\partial \phi}(\mathbf{r}) \right]^2 \right\}. \quad (\text{A10})$$

This can be derived from the relation

$$\frac{\partial \eta_{\text{HD}}}{\partial \alpha}(\mathbf{r}) = 2R_0 n_{0+}(\mathbf{r}), \quad \frac{\partial \eta_{\text{HD}}}{\partial \phi}(\mathbf{r}) = 2R_0 n_{0-}(\mathbf{r}), \quad (\text{A11})$$

with

$$n_{0\pm}(\mathbf{r}) = \frac{1}{2} [\rho_{1\text{D}}(\phi + \alpha(r)) \pm \rho_{1\text{D}}(\phi - \alpha(r))]. \quad (\text{A12})$$

Now using the relations

$$\begin{aligned} \frac{2}{R_0} \frac{\partial n_{0+}}{\partial \alpha}(\mathbf{r}) - \frac{1}{R_0^2} \frac{\partial^2 \eta_{\text{HD}}}{\partial \phi^2}(\mathbf{r}) &= 0, \\ \frac{n_{0+}(\mathbf{r}) \frac{\partial \eta_{\text{HD}}}{\partial \alpha}(\mathbf{r})}{1 - \eta_{\text{HD}}(\mathbf{r})} &= -\frac{\partial}{\partial \alpha} \{n_{0+}(\mathbf{r}) \ln[1 - \eta_{\text{HD}}(\mathbf{r})]\} + \frac{\partial n_{0+}}{\partial \alpha}(\mathbf{r}) \ln[1 - \eta_{\text{HD}}(\mathbf{r})], \\ \frac{\left[\frac{\partial \eta_{\text{HD}}}{\partial \phi}(\mathbf{r}) \right]^2}{1 - \eta_{\text{HD}}(\mathbf{r})} &= -\frac{\partial}{\partial \phi} \left\{ \frac{\partial \eta_{\text{HD}}}{\partial \phi}(\mathbf{r}) \ln[1 - \eta_{\text{HD}}(\mathbf{r})] \right\} + \frac{\partial^2 \eta_{\text{HD}}}{\partial \phi^2}(\mathbf{r}) \ln[1 - \eta_{\text{HD}}(\mathbf{r})] \end{aligned} \quad (\text{A13})$$

we get

$$\begin{aligned} & \frac{2n_{0+}(\mathbf{r}) \frac{\partial \eta_{\text{HD}}(\mathbf{r})}{\partial \alpha}}{R_0[1 - \eta_{\text{HD}}(\mathbf{r})]} - \frac{\left[\frac{\partial \eta_{\text{HD}}(\mathbf{r})}{\partial \phi} \right]^2}{R_0^2[1 - \eta_{\text{HD}}(\mathbf{r})]} \\ &= -\frac{2}{R_0} \frac{\partial}{\partial \alpha} \{n_{0+}(\mathbf{r}) \ln[1 - \eta_{\text{HD}}(\mathbf{r})]\} + \frac{1}{R_0^2} \frac{\partial}{\partial \phi} \left\{ \frac{\partial \eta_{\text{HD}}(\mathbf{r})}{\partial \phi} \ln[1 - \eta_{\text{HD}}(\mathbf{r})] \right\}. \end{aligned} \quad (\text{A14})$$

Next we take into account the periodic condition $\eta_{\text{HD}}(r, \phi) = \eta_{\text{HD}}(r, \phi + 2\pi)$ which implies

$$\int_0^{2\pi} d\phi \frac{\partial}{\partial \phi} \left\{ \frac{\partial \eta_{\text{HD}}(\mathbf{r})}{\partial \phi} \ln[1 - \eta_{\text{HD}}(\mathbf{r})] \right\} = 0. \quad (\text{A15})$$

Eqs. (A10), (A14) and (A15) can be used to give

$$\int_0^{2\pi} d\phi \frac{2R_0^2}{\pi} \frac{\rho_{1\text{D}}(\phi - \alpha(r))\rho_{1\text{D}}(\phi + \alpha(r))}{1 - \eta_{\text{HD}}(\mathbf{r})} = - \int_0^{2\pi} d\phi \frac{R_0}{\pi} \frac{\partial}{\partial \alpha} \{n_{0+}(\mathbf{r}) \ln[1 - \eta_{\text{HD}}(\mathbf{r})]\} \quad (\text{A16})$$

Introducing the change of variable $(r, \phi) \rightarrow (\gamma, \phi)$ and using Eqs. (A7), (A8) and (A16), the excess part of the free-energy (1) can be rewritten as (8).

1. The case $R_0 > R$

Using (9) we have

$$\begin{aligned} & \int_0^\pi d\gamma \frac{\partial \Psi}{\partial \alpha}(\phi, \alpha(\gamma)) \theta^*(\gamma) \left| \frac{d\alpha}{d\gamma}(\gamma) \right| = \int_0^{\gamma_0} d\gamma \frac{\partial \Psi}{\partial \alpha}(\phi, \alpha(\gamma)) (\pi - \theta(\gamma)) \frac{d\alpha}{d\gamma}(\gamma) \\ & + \int_{\gamma_0}^\pi d\gamma \frac{\partial \Psi}{\partial \alpha}(\phi, \alpha(\gamma)) \theta(\gamma) \left(-\frac{d\alpha}{d\gamma}(\gamma) \right) \\ &= [\pi \Psi(\phi, \alpha)]_{\alpha(0)}^{\alpha_0} - \underbrace{\int_0^\pi d\gamma \frac{\partial}{\partial \alpha} [\Psi(\phi, \alpha(\gamma)) \theta(\gamma)] \frac{d\alpha}{d\gamma}(\gamma)}_{=[\Psi(\phi, \alpha) \theta(\alpha)]_{\alpha(0)}^{\alpha(\pi)}=0} + \int_0^\pi d\gamma \Psi(\phi, \alpha(\gamma)) \frac{d\theta}{d\alpha}(\gamma) \frac{d\alpha}{d\gamma}(\gamma) \\ &= \pi \Psi(\phi, \alpha_0) + \int_0^\pi d\gamma \Psi(\phi, \alpha(\gamma)) \frac{d\theta}{d\alpha}(\gamma) \frac{d\alpha}{d\gamma}(\gamma), \end{aligned} \quad (\text{A17})$$

where we have used the change of variable $\int_{\gamma_1}^{\gamma_2} d\gamma T(\phi, \alpha(\gamma)) \frac{d\alpha}{d\gamma}(\gamma) = \int_{\alpha(\gamma_1)}^{\alpha(\gamma_2)} d\alpha T(\phi, \alpha)$ for a general function $T(\phi, \alpha)$ and also that $\alpha(0) = \alpha(\pi) = 0$. Now from (A17) and (8) we can reexpress the excess free energy as

$$\beta \mathcal{F}_{\text{ex}}^{(\text{HD})}[\rho] = \frac{R_0}{\pi} \int_0^{2\pi} d\phi \left\{ \pi \Psi(\phi, \alpha_0) + \int_0^\pi d\gamma \Psi(\phi, \alpha(\gamma)) \left(1 + \frac{d\theta}{d\alpha}(\gamma) \frac{d\alpha}{d\gamma}(\gamma) \right) \right\}. \quad (\text{A18})$$

Further, since $\alpha + \theta + \gamma = \pi$, we have

$$d\gamma + \frac{d\theta}{d\alpha} \frac{d\alpha}{d\gamma} d\gamma = d\alpha \left(\frac{d\gamma}{d\alpha} + \frac{d\theta}{d\alpha} \right) = -d\alpha \quad (\text{A19})$$

and

$$\beta \mathcal{F}_{\text{ex}}^{(\text{HD})}[\rho] = \frac{R_0}{\pi} \int_0^{2\pi} d\phi \left\{ \pi \Psi(\phi, \alpha_0) - \underbrace{\int_{\alpha(0)}^{\alpha(\pi)} d\alpha \Psi(\phi, \alpha)}_{=0} \right\}. \quad (\text{A20})$$

Let us redefine the weighted densities as in (12) and (13) where the index ‘CA’ means that these densities are those on a circular arc of length $2R_0\alpha_0$. Then we have proved that the excess part of the HD free-energy functional reduces to that of hard CA, given by Eq. (10).

2. The case $R_0 < R$

Taking into account (14), Eq. (8) reads

$$\beta \mathcal{F}_{\text{ex}}^{(\text{HD})}[\rho] = \frac{R_0}{\pi} \int_0^{2\pi} d\phi \int_0^\pi d\gamma \left\{ \Psi(\phi, \alpha(\gamma)) - \frac{\partial \Psi}{\partial \alpha}(\phi, \alpha(\gamma)) \theta(\gamma) \frac{d\alpha}{d\gamma}(\gamma) \right\}. \quad (\text{A21})$$

Using

$$\frac{\partial \Psi}{\partial \alpha}(\phi, \alpha) \theta(\gamma) = \frac{\partial}{\partial \alpha} [\Psi(\phi, \alpha) \theta(\gamma)] - \Psi(\phi, \alpha) \frac{d\theta}{d\alpha}(\gamma), \quad (\text{A22})$$

Eq. (A21) becomes

$$\begin{aligned} \beta \mathcal{F}_{\text{ex}}^{(\text{HD})}[\rho] &= \frac{R_0}{\pi} \int_0^{2\pi} d\phi \left[\int_0^\pi d\gamma \Psi(\phi, \alpha(\gamma)) \left(1 + \frac{d\theta}{d\alpha}(\gamma) \frac{d\alpha}{d\gamma}(\gamma) \right) \right. \\ &\quad \left. - \int_0^\pi d\gamma \frac{d\alpha}{d\gamma}(\gamma) \frac{\partial}{\partial \alpha} (\Psi(\phi, \alpha(\gamma)) \theta(\gamma)) \right], \end{aligned} \quad (\text{A23})$$

and, using (A19),

$$\beta \mathcal{F}_{\text{ex}}^{(\text{HD})}[\rho] = \frac{R_0}{\pi} \int_0^{2\pi} d\phi \left\{ - \int_\pi^0 d\alpha \Psi(\phi, \alpha) - \underbrace{[\Psi(\phi, \alpha) \theta(\alpha)]_\pi^0}_{=0} \right\} = \frac{R_0}{\pi} \int_0^{2\pi} d\phi \int_0^\pi d\alpha \Psi(\phi, \alpha), \quad (\text{A24})$$

where we used the fact that the function $\alpha(\gamma)$ has values $\alpha(0) = \pi$ and $\alpha(\pi) = 0$, while the function $\theta(\alpha)$ has values $\theta(0) = \theta(\pi) = 0$ (see Fig. 1). Taking into account now that

$\frac{\partial \eta_{\text{HD}}}{\partial \alpha}(\phi, \alpha) = R_0 [\rho_{1\text{d}}(\phi + \alpha) + \rho_{1\text{d}}(\phi - \alpha)] = 2R_0 n_{0+}(\phi, \alpha)$, we obtain from (A24):

$$\begin{aligned} \beta \mathcal{F}_{\text{ex}}^{(\text{HD})}[\rho] &= -\frac{R_0}{\pi} \int_0^{2\pi} d\phi \int_0^\pi d\alpha \frac{1}{2R_0} \frac{\partial \eta_{\text{HD}}}{\partial \alpha}(\phi, \alpha) \ln[1 - \eta_{\text{HD}}(\phi, \alpha)] \\ &= \frac{1}{2\pi} \int_0^{2\pi} d\phi \int_0^\pi d\alpha \frac{\partial}{\partial \alpha} \{ \eta_{\text{HD}}(\phi, \alpha) + [1 - \eta_{\text{HD}}(\phi, \alpha)] \ln[1 - \eta_{\text{HD}}(\phi, \alpha)] \} \\ &= \frac{1}{2\pi} \int_0^{2\pi} d\phi [\eta_{\text{HD}}(\phi, \alpha) + (1 - \eta_{\text{HD}}(\phi, \alpha)) \ln[1 - \eta_{\text{HD}}(\phi, \alpha)]]_0^\pi. \end{aligned} \quad (\text{A25})$$

Noting that $\eta_{\text{HD}}(\phi, 0) = 0$ and that

$$\eta_{\text{CA}} \equiv \eta_{\text{HD}}(\phi, \pi) = R_0 \int_{\phi-\pi}^{\phi+\pi} d\phi' \rho_{1\text{D}}(\phi') = R_0 \int_{-\pi}^\pi d\phi' \rho_{1\text{D}}(\phi') = 2\pi R_0 \bar{\rho}_{1\text{D}}, \quad (\text{A26})$$

we arrive at (15).

Appendix B: Fourier and Gaussian parameterizations

The expressions for the weighted densities of CR, using the Fourier expansion (36), are

$$\eta_{\text{CR}}(\phi, z) = \eta_0 \left[1 + \sum_{(k,m) \neq (0,0)} s_{km} \chi_1(kN_0\alpha_0) \chi_1\left(\frac{m\pi}{d^*}\right) \cos(kN_0\phi) \cos(qmz) \right], \quad (\text{B1})$$

$$n_0^{(\text{CR})}(\phi, z) = \rho_0 \left[1 + \sum_{(k,m) \neq (0,0)} s_{km} \chi_0(kN_0\alpha_0) \chi_0\left(\frac{m\pi}{d^*}\right) \cos(kN_0\phi) \cos(qmz) \right], \quad (\text{B2})$$

$$n_{1,\perp}^{(\text{CR})}(\phi, z) = \frac{\eta_0}{L} \left[1 + \sum_{(k,m) \neq (0,0)} s_{km} \chi_1(kN_0\alpha_0) \chi_0\left(\frac{m\pi}{d^*}\right) \cos(kN_0\phi) \cos(qmz) \right], \quad (\text{B3})$$

$$n_{1,\parallel}^{(\text{CR})}(\phi, z) = \rho_0 L \left[1 + \sum_{(k,m) \neq (0,0)} s_{km} \chi_0(kN_0\alpha_0) \chi_0\left(\frac{m\pi}{d^*}\right) \cos(kN_0\phi) \cos(qmz) \right], \quad (\text{B4})$$

where $\eta_0 = 2\rho_0 R_0 \alpha_0 L$ is the mean packing fraction, $d^* = d/L$ is the z -period in reduced units, and $\chi_0(x) \equiv \cos x$, $\chi_1(x) \equiv \sin x/x$.

Within the Gaussian parameterization (37), the free-energy density-functional of CR can

be computed as

$$\begin{aligned} \frac{\beta \mathcal{F}_{\text{CR}}[\rho]a}{2\pi R_0 \mathcal{L}} = & \eta_0 \left\{ \ln \left[\frac{\eta_0 \sqrt{\Lambda_{\perp}^* \Lambda_{\parallel}^*}}{\pi a} \right] - 1 + \frac{2}{\sqrt{\pi}} \int_0^\infty dt e^{-t^2} \ln \left\{ \prod_{\tau=\perp, \parallel} \left[\sum_k \exp \left(- \left(t - k \sqrt{\Lambda_{\tau}^*} \right)^2 \right) \right] \right\} \right. \\ & \left. + \frac{1}{\pi} \int_0^\infty dt_1 e^{-t_1^2} \int_0^\infty dz e^{-t_2^2} T \left(\frac{t_1}{\sqrt{\Lambda_{\perp}^*} R_0}, \frac{t_2}{\sqrt{\Lambda_{\parallel}^*}} \right) \right\}. \end{aligned} \quad (\text{B5})$$

where $a = 2R_0\alpha_0 L$ is the particle area and we have defined $\Lambda_{\perp}^* \equiv \Lambda(\phi_0^*)^2$ [with $\phi_0^* = \pi/(N_0\alpha_0)$], $\Lambda_{\parallel}^* \equiv \Lambda(d^*)^2$, and

$$T(\phi, z) = \sum_{\tau_1, \tau_2=\pm} H(\phi_{\tau_1}, z_{\tau_2}), \quad H(\phi, z) = -\ln[1 - \eta_{\text{CR}}(\phi, z)] + \frac{\eta_{\text{CR}}(\phi, z)}{1 - \eta_{\text{CR}}(\phi, z)}, \quad (\text{B6})$$

with $\phi_{\pm} = \phi \pm \alpha_0$, $z = z \pm L/2$, and $\eta_{\text{CR}}(\phi, z) = (1 - \nu)\zeta_{1\perp}(\phi)\zeta_{1\parallel}(z)$. We have used the notation

$$\begin{aligned} \zeta_{1\perp} \left(\frac{t_1}{\sqrt{\Lambda_{\perp}^*} R_0} \right) &= \frac{1}{2} \sum_k \left\{ \text{erf} \left[t_1 + \sqrt{\Lambda_{\perp}^*} \left(\frac{1}{2\phi_0^*} - k \right) \right] - \text{erf} \left[t_1 - \sqrt{\Lambda_{\perp}^*} \left(\frac{1}{2\phi_0^*} + k \right) \right] \right\}, \\ \zeta_{1\parallel} \left(\frac{t_2}{\sqrt{\Lambda_{\parallel}^*}} \right) &= \frac{1}{2} \sum_k \left\{ \text{erf} \left[t_2 + \sqrt{\Lambda_{\parallel}^*} \left(\frac{1}{2d^*} - k \right) \right] - \text{erf} \left[t_2 - \sqrt{\Lambda_{\parallel}^*} \left(\frac{1}{2d^*} + k \right) \right] \right\}, \end{aligned} \quad (\text{B7})$$

with $\text{erf}(x)$ the error function.

Appendix C: DF for spherical lenses

The correct dimensional cross-over of HS confined on a spherical surface means the following: When the density profile of HS is restricted to be on a spherical surface of radius R_0 , $\rho_{3\text{D}}(r, \hat{\Omega}) = \rho_{2\text{D}}(\hat{\Omega})\delta(R_0 - r)$, where (r, θ, ϕ) are the radius and the angles of spherical coordinates, while $\hat{\Omega}(\theta, \phi) = (\sin \theta \cos \phi, \sin \theta \sin \phi, \cos \theta)$ is the unit vector in the radial direction, we should obtain

$$\beta \mathcal{F}_{\text{ex}}^{(\text{HS})}[\rho] \rightarrow \beta \mathcal{F}_{\text{ex}}^{(\text{SL})}[\rho] = R_0^2 \int d\hat{\Omega} \Phi_{2\text{D}}^{(\text{SL})}(\hat{\Omega}), \quad (\text{C1})$$

which results in a dimensionally-reduced density functional for spherical lenses (SL), where $d\hat{\Omega} = d\phi d\theta \sin \theta$ is the solid-angle element. The expression for $\Phi_{2\text{D}}(\hat{\Omega})$ is the same as in (2),

with the weighted densities now defined as

$$n_0^{(\text{SL})}(\hat{\Omega}) = \frac{R_0}{2\pi R} \int d\hat{\Omega}_1 \rho_{2\text{D}}(\hat{\Omega}_1) \delta(\alpha_0 - \gamma(\hat{\Omega}, \hat{\Omega}_1)), \quad (\text{C2})$$

$$\eta_{\text{SL}}(\hat{\Omega}) = R_0^2 \int d\hat{\Omega}_1 \rho_{2\text{D}}(\hat{\Omega}_1) \Theta(\alpha_0 - \gamma(\hat{\Omega}, \hat{\Omega}_1)), \quad (\text{C3})$$

$$N_{\text{SL}}(\hat{\Omega}) = \left(\frac{R_0}{2\pi R}\right)^2 \int d\hat{\Omega}_1 \int d\hat{\Omega}_2 \rho_{2\text{D}}(\hat{\Omega}_1) \rho_{2\text{D}}(\hat{\Omega}_2) \delta(\alpha_0 - \gamma(\hat{\Omega}, \hat{\Omega}_1)) \delta(\alpha_0 - \gamma(\hat{\Omega}, \hat{\Omega}_2)) \\ \times \mathcal{K}\left(\frac{R\gamma(\hat{\Omega}_1, \hat{\Omega}_2)}{\alpha_0}\right), \quad (\text{C4})$$

where $\alpha_0 = \sin^{-1}(R/R_0)$ and we have used the notations

$$\cos \gamma(\hat{\Omega}, \hat{\Omega}_i) = \sin \theta \sin \theta_i \cos(\phi - \phi_i) + \cos \theta \cos \theta_i, \quad i = 1, 2, \quad (\text{C5})$$

$$\cos \gamma(\hat{\Omega}_1, \hat{\Omega}_2) = \sin \theta_1 \sin \theta_2 \cos(\phi_1 - \phi_2) + \cos \theta_1 \cos \theta_2, \quad (\text{C6})$$

which define the angles between the unit vectors $\hat{\Omega}$ and $\hat{\Omega}_i$ and $\hat{\Omega}_1$ and $\hat{\Omega}_2$ respectively. The kernel $\mathcal{K}(r)$ is that defined in Eq. (6). The condition $\rho_{2\text{D}}(\theta + 2\pi, \phi + 2\pi)$ should be imposed, as the density profile is now a periodic function of ϕ and θ .

Acknowledgments

We acknowledge financial support from Comunidad Autónoma de Madrid (Spain) under the R&D Programme of Activities MODELICO-CM/S2009ESP-1691, and from MINECO (Spain) under grants MOSAICO, FIS2010-22047-C01 and FIS2010-22047-C04.

-
- [1] D. R. Nelson, *Defects and Geometry in Condensed Matter Physics* (Cambridge University Press, Cambridge 2002).
 - [2] D. R. Nelson, Phys. Rev. B **28**, 5515 (1983).
 - [3] M. Bowick, D. R. Nelson, and A. Travesset, Phys. Rev. B **62**, 8738 (2000).
 - [4] A. R. Bausch, M. J. Bowick, A. Cacciuto, A. D. Dinsmore, M. F. Hsu, D. R. Nelson, M. G. Nikolaides, A. Travesset and D. A. Weitz, Science **299**, 1716 (2003).
 - [5] J. Lidmar, L. Mirny and D. R. Nelson, Phys. Rev. E **68**, 051910 (2003).
 - [6] S. Sachdev and D. R. Nelson, J. Phys. C **17**, 5473 (1984).
 - [7] A. D. Dinsmore, D. T. Wong, P. Nelson and A. G. Yodh, Phys. Rev. Lett. **80**, 409 (1998).

- [8] A. Amir, J. Paulose and D. R. Nelson, arXiv:1301.4226v1 [cond-mat.soft].
- [9] J. Dzubiella, M. Schmidt and H. Löwen, Phys. Rev. E **62**, 5081 (2000).
- [10] A. González, J. A. White, F. L. Román and S. Velasco, J. Chem. Phys. **125**, 064703 (2006).
- [11] T. Franosch, S. Lang and R. Schilling, Phys. rev. Lett. **109**, 240601 (2012).
- [12] D. de las Heras, E. Velasco and L. Mederos, Phys. Rev. Lett. **94**, 17801 (2005).
- [13] D. de las Heras, E. Velasco and L. Mederos, Phys. Rev. E **74**, 011709 (2006).
- [14] A. Mughal, H. K. Chan and D. Weaire, Phys. Rev. Lett. **106**, 115704 (2011).
- [15] Y. Rosenfeld, M. Schmidt, H. Löwen, and P. Tarazona, Phys. Rev. E **55**, 4245 (1997).
- [16] P. Tarazona and Y. Rosenfeld, Phys. Rev. E **55**, 4245 (1997).
- [17] J. A. Cuesta and Y. Martínez-Ratón, Phys. Rev. Lett. **78**, 3681 (1997).
- [18] Y. Martínez-Ratón, J. A. Capitán and J. A. Cuesta, Phys. Rev. E **77**, 051205 (2008).
- [19] A. V. Kityk and P. Huber, Appl. Phys. Lett. **97**, 153124 (2010).
- [20] S. Belli, M. Dijkstra and R. van Roij, J. Chem. Phys. **137**, 124506 (2012).
- [21] W. G. Hoover, C. G. Hoover and M. N. Bannermann, J. Stat. Phys. **136**, 715 (2009).
- [22] J. A. Capitán, Y. Martínez-Ratón and J. A. Cuesta, J. Chem. Phys **128**, 194901 (2008).
- [23] A. Amir and D. Nelson, PNAS **109**, 9833 (2012).